Available online at www.sciencedirect.com
ScienceDirect
International Journal of Hydrogen Energy 32 (2007) 3471–3485
International Journal of HYDROGEN ENERGY
www.elsevier.com/locate/ijhydene

The ignition, combustion and flame structure of carbon monoxide/hydrogen mixtures. Note 1: Detailed kinetic modeling of syngas combustion also in presence of nitrogen compounds

A. Frassoldati, T. Faravelli, E. Ranzi*

CMIC Dipartimento di Chimica, Materiali e Ingegneria Chimica, Politecnico di Milano, Piazza Leonardo da Vinci 32, 20133 Milano, Italy

Received 28 November 2006; received in revised form 18 January 2007; accepted 18 January 2007
Available online 9 March 2007

Abstract

The kinetic characterization of the H_2/CO system is of interest right now due mainly to its role in sustainable combustion processes. The aim of this paper is to revise and validate a detailed kinetic model of hydrogen and carbon monoxide mixture combustion with particular focus not only on NO_x formation but also on interactions with nitrogen species. Model predictions and experimental measurements are discussed and compared across a wide range of operating conditions. This study moves from the detailed analysis of species profiles in syngas oxidation in flow reactor and laminar premixed flames to global combustion properties (ignition delay times and laminar flame speeds) by referring to a large set of literature data. According to recent literature, the validation of the kinetic scheme confirmed there was a need to slightly modify the kinetic parameters of two relevant CO_2 formation reactions ($CO + OH = CO_2 + H$ and $CO + O + M = CO_2 + M$) and of reaction $HONO + OH = NO_2 + H_2O$.

Keywords: Syngas kinetics; Combustion modeling; NO_x formation; Flame speed; Ignition delay; Syngas flames

1. Introduction

Synthesis gas (syngas) is a mixture of hydrogen and carbon monoxide and can be obtained from natural gas, coal, petroleum, biomass and even organic waste [1]. Syngas can also yield a wide range of chemicals. For instance, almost all hydrogen gas, for which there is a rapidly growing demand in industry, is manufactured from syngas. Methanol synthesis and Fischer–Tropsch syntheses remain the largest consumers of syngas. Syngas is also the main source of carbon monoxide which is used in a great number of carbonylation reactions. However syngas is increasingly seen as a source of environmentally clean fuels too and has the potential to become a major fuel in the production of essentially pollution-free energy. There are many advantages to using syngas as a fuel: generally speaking, it is less expensive and can be used for clean combustion resulting in a significant reduction in pollutant emissions. One promising application of syngas as a direct fuel in Integrated Gasification Combined Cycle (IGCC) units used to generate electricity from coal, petroleum coke or heavy residuals. Over the next 10 years the quantity of syngas used for this may rise to near the amount used for other purposes. Syngas can also be employed as a supplemental fuel to reduce the consumption of other fuels, such as pulverized coal and fuel oil [2]. In addition to this, it has the potential as a reburning fuel to reduce NO_x emissions.

There is renewed interest at present in syngas chemistry for all of the abovementioned reasons, not simply because of its primary role in the hierarchal structure of hydrocarbon fuel combustion but also due to direct interest in this fuel. Syngas, produced by biomass and coal gasification is a mixture of carbon monoxide and hydrogen which also contains methane, carbon dioxide and nitrogen. The internal composition of syngas fuels can vary greatly depending on the source and the processing technique; the volumetric H_2/CO ratio usually varies from 0.33 to 40, diluent gases range from 4% to 51%, and water too can vary from 0% to 40% [3].

* Corresponding author. Fax: +39 02 70638173.
E-mail address: eliseo.ranzi@polimi.it (E. Ranzi).

0360-3199/$ - see front matter © 2007 International Association for Hydrogen Energy. Published by Elsevier Ltd. All rights reserved.
doi:10.1016/j.ijhydene.2007.01.011

Proper kinetic characterization of the H_2/CO system is also of great importance due to the latter's role in the development of advanced combustion technologies such as IGCC. As already mentioned, IGCC is an emerging clean coal technology for power generation. The first step in the IGCC system is the gasification of coal to form syngas mixtures. The subsequent separation of pollutants and sequestration of CO_2 from syngas before combustion makes this gaseous fuel combustion in combined cycle plants both clean and efficient whilst helping to utilize vast reserves of coal [4]. A primary area for IGCC development with high potential for improving plant efficiencies is in syngas turbine design [5]. In addition to this, $H_2/CO/N_2$ mixtures, which are obtained by reforming hydrocarbon fuels, have also been proposed and studied as a means of reducing SI engine cold start emissions [6–8].

The variability in syngas composition substantially modifies steady state and dynamic combustion behavior from one syngas to the next. Thus, not are only combustion instabilities, blowoff and flashback are influenced by syngas composition but pollutant emissions and flame structures can vary significantly too. This is particularly important in the case of gas turbines because these devices are usually highly optimized to meet low emissions levels. Blowout is a concern in low emission combustors which often operate very near the blowout limits. Flashback, that is upstream flame propagation, is also critical for these high flame speed fuels with high hydrogen levels. As a consequence of the large variability of syngas composition, a combustion system designed to operate reliably with one low hydrogen syngas may need to be redesigned to operate satisfactorily with a higher hydrogen-content fuel.

It is mainly for this reason that so many recent kinetic studies have been devoted to improving the characterization of the combustion behavior of H_2/CO mixtures [4,9–12] both from an experimental and a theoretical point of view.

The high temperatures involved in hydrogen combustion can lead to high NO_x emissions. Consequently, the current approach is to fire syngas with high levels of N_2 or steam dilution [13]. As already pointed out, lean premixed turbine operation can overcome concerns regarding high emissions but relevant safety issues must be considered and their optimal design claims for very reliable kinetic models. The availability of comprehensive kinetic mechanisms capable of coping with extensive variations in operating conditions should be a significant advance in view of the development of syngas combustion-based clean technologies [4].

We recently revised the H_2 oxidation mechanism [9] and in this paper we extend this kinetic analysis to verifying H_2/CO model predictions by comparing them also with recent experimental data obtained principally under high-pressure conditions. Particular attention was focused on operating conditions relevant to gas turbine applications and the model was systematically validated against an overall set of experimental measurements covering a wide range of operating conditions. The upgraded H_2/CO kinetic model includes all the most recent and accurate thermodynamic and kinetic estimates.

The interaction of the combustion system with pollutant species (NO_x) and nitrogen components is also accounted for and included in this kinetic study. In fact, not only can syngas obtained from coal and biomasses gasification easily contain trace amounts of nitrogen species [2] but NO_x is also often present in vitiated airstreams and in re-circulating flue gases.

2. Kinetic mechanism

The revised and upgraded reaction mechanism of syngas pyrolysis and combustion is reported in Table 1 while the thermodynamic data are summarized in Table 2. These data and transport properties were taken from the CHEMKIN Database [14] with improved values for OH and HO_2 formation enthalpy [9]. Reverse rate constants are calculated via forward rates and equilibrium constants. The scheme consists of 32 elementary reactions and several modifications were made to the previous kinetic model proposed by Ranzi et al. [15]. The H_2/CO_2 submechanism consists of 20 reversible reactions [9]. The extension to syngas requires only three new species (CO, CO_2 and HCO) and 12 new reactions.

As recently discussed by Davis [10], the reaction $CO + OH = CO_2 + H$ is the critical step and its rate constant does merit special attention. The crucial role of this reaction in hydrocarbon combustion is mainly due to the significant heat released during CO to CO_2 conversion. Fig. 1 reports and compares experimental measurements [16,17] with different rate expressions reported in the literature [10,17,16]. This reaction was experimentally studied by Wooldridge et al. [18,19] who suggested new rate coefficients on the basis of both the infrared absorption of CO_2 and the UV laser absorption of OH. This rate expression is in close agreement with the compilation of experimental measurements recently discussed in the literature [16,17].

Davis et al. [10] used the sum of two modified Arrhenius expressions to more accurately describe the high temperature data of Wooldridge et al. [18] and of Golden et al. [20]. Similarly, a combination of two expressions was used by Joshi and Wang [17] while three expressions were combined by Sun et al. [21]. This is justified by the complexity of the CO+OH reaction and the difficulty in describing this reaction using a single Arrhenius expression over an extended temperature range. The CO+OH reactions proceed both directly and through the chemically activated complex HOCO [17]. Consequently, two reaction channels and two rate expressions explain the complex temperature dependence of this reaction more accurately. A single rate equation cannot satisfactorily represent the available data over the entire temperature range. As clearly shown in Fig. 1, the rate constants suggested by Davis et al. [10] agree with the experimental measurements from low to high temperatures, and as a result, these values have been selected and reported in Table 1.

CO to CO_2 conversion can also proceed through the recombination reaction $CO + O + M = CO_2 + M$, mainly at high pressures and/or in anhydrous systems. Fig. 2 shows the wide scatter of rate constants as reported in the literature [23–32] for the low-pressure expression, together with the suggested fit for the modified Arrhenius expression: $k = 2.07 \times 10^{20} \times T^{-3.34} \times \exp(-7160/RT)$ [$m^6/kmol^2/s$]. This expression is combined

Table 1
$CO/H_2/O_2$ mechanism with rate coefficients in the form $k = A \cdot T^n \cdot \exp(-E_a/RT)$

	Reaction	A	n	E_a	Source
1	$H + O_2 = OH + O$	2.21E + 11	0	16 650	[9]
2	$O + H_2 = OH + H$	4.33E + 10	0	10 000	[9]
3	$H + O_2 + [M] = HO_2 + [M]$	4.65E + 09	−0.8	0	[9]
Low-pressure limit:		7.00E + 11	0.4	0	[9]
Troe parameters: 0.5, $1E-30$ $1E+30$					
Enhanced third-body efficiencies: $H_2O = 18.0$, $H_2 = 2.5$, $N_2 = 1.26$, $O_2 = 0$, Ar = 0.8, He = 0.8, CO = 1.2, $CO_2 = 2.4$					
	$H + O_2 + O_2 = HO_2 + O_2$	8.90E + 08	0	−2822	[9]
4	$OH + HO_2 = H_2O + O_2$	5.00E + 10	0	1000	[9]
5	$H + HO_2 = OH + OH$	2.50E + 11	0	1900	[9]
6	$O + HO_2 = O_2 + OH$	3.25E + 10	0	0	[9]
7	$OH + OH = O + H_2O$	7.36E + 09	0	1100	[9]
8	$H_2 + [M] = H + H + [M]$	2.23E + 11	0	96 081	[9]
Enhanced third-body efficiencies:$H_2O = 12.0$, $H_2 = 2.5$, CO = 1.9, $CO_2 = 3.8$, Ar = 0.5, He = 0.5					
9	$O_2 + [M] = O + O + [M]$	1.55E + 11	0	115 120	[9]
Enhanced third-body efficiencies:$H_2O = 12.0$, $H_2 = 2.5$, CO = 1.9, $CO_2 = 3.8$, Ar = 0.2, He = 0.2					
10	$H + OH + [M] = H_2O + [M]$	4.50E + 16	−2	0	[9]
Enhanced third-body efficiencies: $H_2O = 16.0$, $H_2 = 2.0$, $CO_2 = 1.9$					
11	$H + HO_2 = H_2 + O_2$	2.50E + 10	0	700	[9]
12	$HO_2 + HO_2 = H_2O_2 + O_2$	2.11E + 09	0	0	[9]
13	$OH + OH + [M] = H_2O_2 + [M]$	7.40E + 10	−0.37	0	[9]
Low-pressure limit:		2.30E + 12	−0.9	−1700	
Troe parameters: 0.7346, 94.00, 1756, 5182					
Enhanced third-body efficiencies: $H_2O = 6$, $H_2 = 2$, CO = 1.5, $CO_2 = 2.0$, $CH_4 = 2.0$, $C_2H_6 = 3.0$, Ar = 0.7, He = 0.7					
14	$O + OH + [M] = HO_2 + [M]$	1.00E + 10	0	0	[9]
15	$H + H_2O = H_2 + OH$	4.00E + 07	1	19 000	[9]
16	$H_2O_2 + H = H_2O + OH$	2.41E + 10	0	3970	[9]
17	$H_2O_2 + H = H_2 + HO_2$	6.03E + 10	0	7950	[9]
18	$HO_2 + H_2O \rightarrow H_2O_2 + OH$	5.39E + 05	2	28 780	[9]
19	$OH + H_2O_2 \rightarrow H_2O + HO_2$	3.20E + 05	2	−4170	[9]
20	$O + H_2O_2 \rightarrow OH + HO_2$	1.08E + 06	2	−1657	[9]
21	$CO + O + [M] = CO_2 + [M]$	9.64E + 07	0	3800	[22]
Low-pressure limit:		2.07E + 20	−3.34	7610	[33]
Enhanced third-body efficiencies: $H_2O = 12.0$, $H_2 = 2.0$, CO = 1.5, $CO_2 = 2.0$, Ar = 0.5					
22	$CO + OH = CO_2 + H$	9.60E + 08	0.14	7352	[10]
		7.32E + 07	0.03	−16	
23	$CO + HO_2 = CO_2 + OH$	3.01E + 10	0	23 000	[32]
24	$CO + H_2O = CO_2 + H_2$	2.00E + 08	0	38 000	[15]
25	$O_2 + CO = CO_2 + O$	2.53E + 09	0	47 700	[23]
26	$HCO + [M] = CO + H + [M]$	1.20E + 14	−1	17 000	[64]×0.65
Enhanced third-body efficiencies: $H_2O = 5.0$, $H_2 = 1.9$, CO = 1.9, $CO_2 = 3.0$					
27	$HCO + O = CO_2 + H$	3.00E + 10	0	0	[23]
28	$HCO + H = H_2 + CO$	1.00E + 11	0	0	[65]
29	$HCO + OH = H_2O + CO$	5.00E + 10	0	0	[25]
30	$HCO + HO_2 = H_2O_2 + CO$	4.00E + 08	0	0	[15]
31	$O_2 + HCO = HO_2 + CO$	1.00E + 09	0	0	[15]
32	$HCO + HO_2 \Rightarrow H + OH + CO_2$	3.00E + 10	0	0	[25]

A units: mol/l/s/K; E_a units: cal/mol.

with the high-pressure parameters of Kondratiev [33] using the Lindemann fit, as already suggested by Allen et al. [34]. This high-pressure value is about 2–3 times faster than the one suggested by Troe [35]. Moreover, the rate parameters of reaction $CO + HO_2 = CO_2 + OH$ were slightly modified according to the indication of Mueller et al. [32], in order to better describe the syngas reactivity at low temperatures and high pressures. Nitrogen chemistry and kinetics have been discussed in recent papers [9,36,37]. This kinetic model is coupled in this case with the syngas model, and the combined H_2–CO–NO_x kinetic scheme is systematically compared to a wide range of experimental data, including flow and stirred reactors as well as

Table 2
ΔH_f (298.15 K), S (298.15 K), and Cp (T) for species considered in the $CO/H_2/O_2$reaction mechanism

Species	ΔH_f	S	Cp (300 K)	Cp (1000 K)	Cp(2000 K)
N_2	0	45.816	6.949	7.830	8.601
H_2	0	31.256	6.902	7.209	8.183
O_2	0	49.050	7.010	8.350	9.032
H_2O	−57.80	45.154	7.999	9.875	12.224
H_2O_2	−32.53	55.725	10.416	15.213	17.878
OH	8.91	43.978	6.947	7.341	8.213
H	52.099	27.422	4.968	4.968	4.968
O	59.56	38.500	5.232	4.999	4.976
HO_2	3.000	54.809	8.349	11.380	13.321
CO	−26.420	−26.406	47.259	6.950	7.948
CO_2	−94.061	−94.010	51.140	8.910	12.993
HCO	10.401	10.395	53.716	8.245	11.521

Units are cal/mol/K for S and Cp, and kcal/mol for ΔH_f.

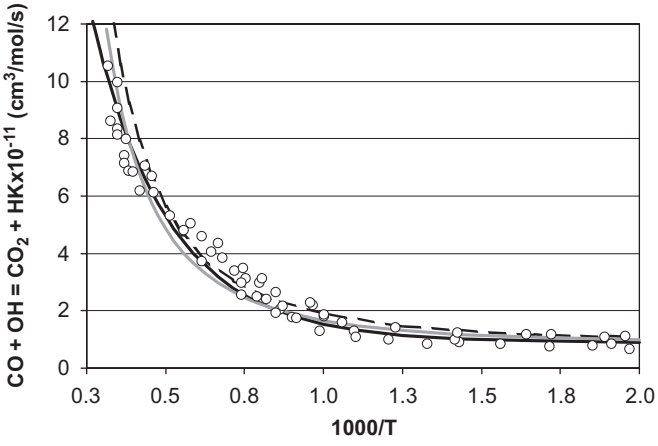

Fig. 1. Rate constant of reaction CO+OH=CO_2+H. Comparison of suggested values of [10] (solid, black line), Joshi and Wang [17] (gray line) and Sun et al. [21] (dashed line) with experimental measurements [16] (symbols).

laminar and turbulent flames. As a result of this validation, only the reaction HONO + OH = NO_2 + H_2O was updated to improve model predictions under the specific conditions of NO_x addition to the syngas combustion.

The whole set of data discussed in this note is reported in Table 3 and includes stirred and flow reactors, shock tubes and premixed flames. Further comparisons with experimental measurements relating to turbulent diffusion flames of syngas, including NO_x formation [38,39], are discussed in the Note 2 of this work.

For the sake of clarity, these comparisons are divided in two separate paragraphs. The H_2–CO model is discussed first and the data involving nitrogen chemistry and/or NO_x formation are analyzed later.

DSMOKE code was used to solve the equation systems of shock tube and ideal reactors [40]. PREMIX and OPPDIF Sandia codes [41,42] and the CHEMKIN transport package [14] were used for flame simulations. Multicomponent diffusion and thermal diffusion are included since they are important in syngas combustion, due to the hydrogen content.

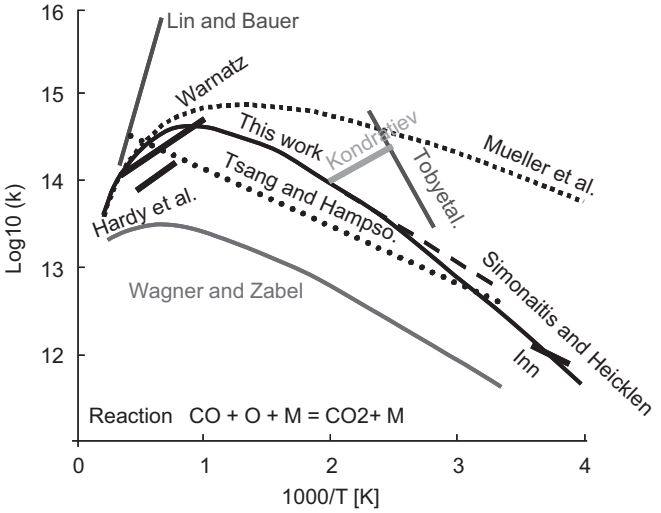

Fig. 2. Reaction CO + O + M = CO_2 + M. Comparison of the low-pressure rate constants suggested by different authors [23–32] and the one adopted in this paper (K units: mol cm^3 s).

3. Validation of the H_2-CO kinetic scheme

3.1. Flow and JSR reactors

Yetter et al. [43,44] studied moist CO oxidation in a plug flow reactor at 1 atm and ~1030 K in nearly adiabatic conditions. Time shifting was used to take into account the non-ideal mixing at the inlet, as suggested by Yetter et al. [43,44]. Fig. 3 shows a comparison between experimental measurements and model results. The predicted profiles of the different species agree well with the measurements for both the conditions analyzed.

The effect of pressure on CO reactivity in a diluted O_2/H_2O mixture is presented in Fig. 4a. At 1040 K and up to 3.46 atm, the system exhibits an induction period followed by rapid oxidation, while at higher pressures, CO conversion drops significantly. The sensitivity analysis presented in Fig. 4b clearly shows that the system's reactivity is mainly ruled by the competition between the chain branching H + O_2 and the chain terminating paths H + O_2 + M. The reaction CO + O + M = CO_2 + M is always significant, especially at 3–5 atm. It is worth noting that the new kinetic parameters allow close agreement with experimental measurements in these conditions. Similarly, the $CO/H_2/N_2O$ ignition delay measurements made by Dean et al. [45] are highly sensitive to this reaction as discussed in the next paragraph.

The moist oxidation of CO in a nearly atmospheric plug flow reactor at 800–1500 K was studied by Alzueta et al. [46] to evaluate the effect of SO_2 addition. Pure CO oxidation experiments with N_2 dilution were performed for reference purposes and those measurements are compared to model predictions in Fig. 5. Three different conditions were analyzed:

(a) Very lean conditions: CO = 100 ppm, O_2 = 96 000 ppm, H_2O = 0.5%, τ = 198 [K]/T [s].

Table 3
Experimental measurements on $CO/H_2/NO_x$ systems studied in this paper

Experiment	Mixture	Temperature (K)	Φ	Pressure (atm)	Figures	Source
Plug flow reactor	$CO/O_2/H_2O/N_2$ ($CO/H_2O = 1.56$–1.73)	1032–1033	0.7–1.1	1	3	[43]
	$CO/O_2/H_2O/N_2$ ($CO/H_2O = 1.55$)	1040	1	1–9.6	4	[44]
	$CO/O_2/H_2O/N_2$ ($CO/H_2O = 0.02$–0.08)	850–1400	0.0005–1.25	1.05	5	[46]
	$CO/O_2/H_2O/N_2$ ($H_2O = 1$–9% NO = 0–1430 ppm)	800–1200	0.006	1.05	18	[47]
	$NO/NH_3/O_2/N_2+$ $CO/H_2 = 0$–∞ (NO = 0–2500 ppm) (NH_3 = 1000 ppm)	1273	0–∞	1	19–20	[63]
Stirred reactor	$CO/H_2/O_2/N_2$ ($CO/H_2 = 1$ NO = 0–1000 ppm)	850–1350	0.1–2	1	17	[48]
Ignition delay times	$CO/H_2/O_2/Ar$ ($CO/H_2 = 0$–3)	900–1500	1	10	7	[50]
	$CO/H_2/Air$ ($CO/H_2 = 0.25$–19)	890–1285	0.5	1.05–15	8	[11,51]
	$CO/H_2/O_2/Ar$ ($CO/H_2 = 67$–243)	2000–2850	1.65–6.1	1.2–2.2	9	[45]
	$CO/H_2/N_2O/Ar$ ($CO/H_2 = 60$–245)	2000–2850	3–11.6	1.2–2.2	10	[45]
	$CO/H_2/O_2/Ar$ ($CO/H_2 \cong 2.5$)	1100–1450	0.5–1	256–450	6	[49]
Flame speeds	$CO/H_2/Air$ ($CO/H_2 = 1$–99)	298	0.3–6	1	13a	[21,54–57]
	$CO/H_2/Air$ ($CO/H_2 = 1$–∞)	298	1	1	13b	[55]
	$CO/H_2/Air$ $CO/H_2/O_2/He$ ($CO/H_2 = 1$–19)	298	05–05	1–2 5–10	14	[21]
	$CO/H_2/CO_2/Air$ ($CO/H_2 = 8.86$)	298	08–2.3	1	15a	[58]
	$CO/H_2/O_2/N_2/H_2O$ ($CO/H_2 = 64.8$)	298	04–6.6	1	15b	[59]
Ignition in a counter-flow flame	$CO/H_2/Air$ ($CO/H_2 = 0$–∞)	600–2000	0–∞	1	12	[53]
Premixed flame	$CO/H_2/N_2/O/Ar$ ($CO/H_2 = 0.32$)	600–2000	1.2	0.039	16	[60]

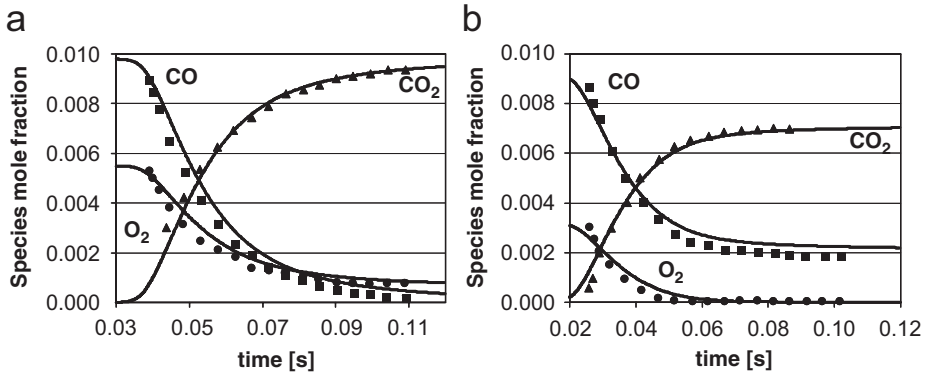

Fig. 3. CO conversion in a plug flow reactor [43]. Panel (a). CO = 0.98%, O_2 = 0.55%, H_2O = 0.565%, balance N_2. Panel (b). CO = 0.92%, O_2 = 0.32%, H_2O = 0.59%, balance N_2. Comparison between predicted (lines) and measured (symbols) species profiles.

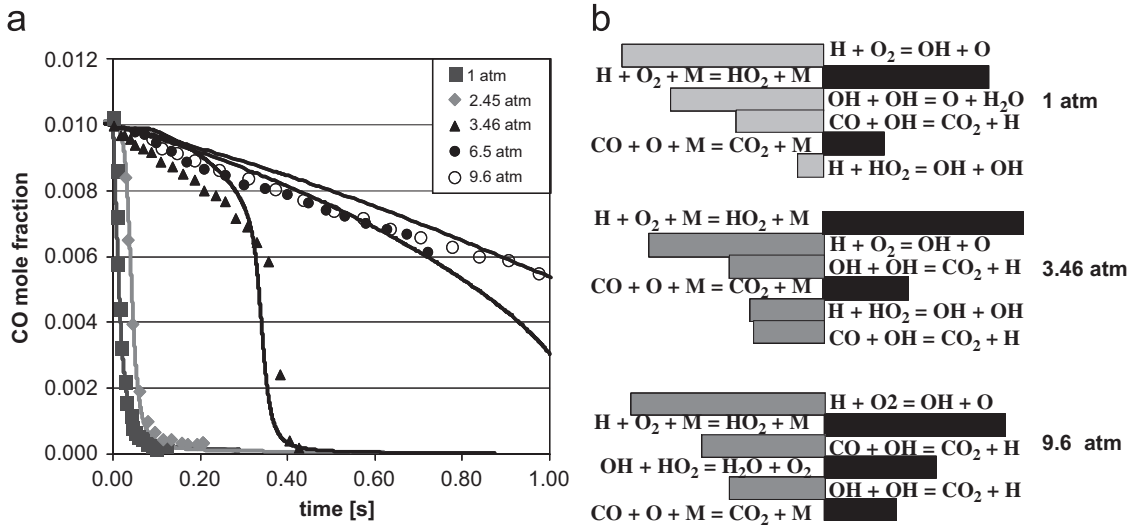

Fig. 4. Pressure effect on CO conversion in a plug flow reactor at 1040 K (CO = 1.01%, O_2 = 0.5%, H_2O = 0.65%, balance N_2) [44]. Panel (a). Comparison between predicted (lines) and measured (symbols) CO profiles. Panel (b). Maximum sensitivity coefficients of [CO]. Dark bars correspond to positive sensitivity cofficients.

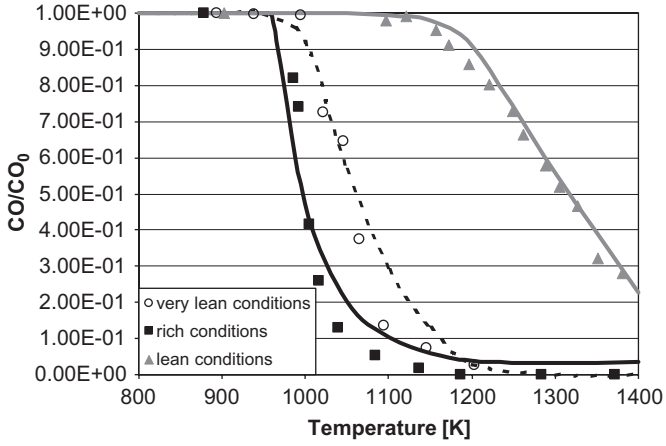

Fig. 5. CO conversion in a plug flow reactor under rich (squares), lean (triangles) and very lean (circles) conditions. Comparison between experimental data (symbols) [46] and model predictions (lines).

(b) Lean conditions: CO = 107 ppm, O_2 = 112 ppm, H_2O = 0.5%, τ = 201 [K]/T [s].
(c) Rich conditions: CO = 1009 ppm, O_2 = 403 ppm, H_2O = 1.3%, τ = 188 [K]/T [s].

The model properly predicts conversion and induction times under these conditions too. A sensitivity analysis, performed both in rich and very lean conditions, revealed that the reactivity of the system is always controlled by the competition between chain branching ($H + O_2 = OH + O$) and the slow chain propagation ($H + O_2 + M = HO_2 + M$) reactions followed by CO oxidation by OH radicals.

Similar experiments were performed in the past with syngas mixtures in a plug flow reactor by Glarborg et al. [47] and, more recently, in a jet stirred reactor at various equivalence ratios by Dagaut et al. [48]. The main purpose of both these kinetic studies was to analyze the effect of NO addition to H_2/CO mixtures. For this reason the comparisons between experimental data and model predictions are presented and discussed in Figs. 16 and 17 in the next paragraph in which nitrogen species chemistry is also analyzed.

3.2. Shock tube device and ignition delay times

Sivaramakrishnan et al. [49] recently presented very interesting data obtained at extremely high pressures in the shock tube device at UIC. As previously mentioned, one of the main focuses of this kinetic work is to accurately verify the model predictions at high pressures. The comparisons between model results and experimental measurements reported in Fig. 6 refer to two different sets of experiments, at 256 and 450 atm, respectively at Φ = 0.5 and 1. As shown in the figure, the model

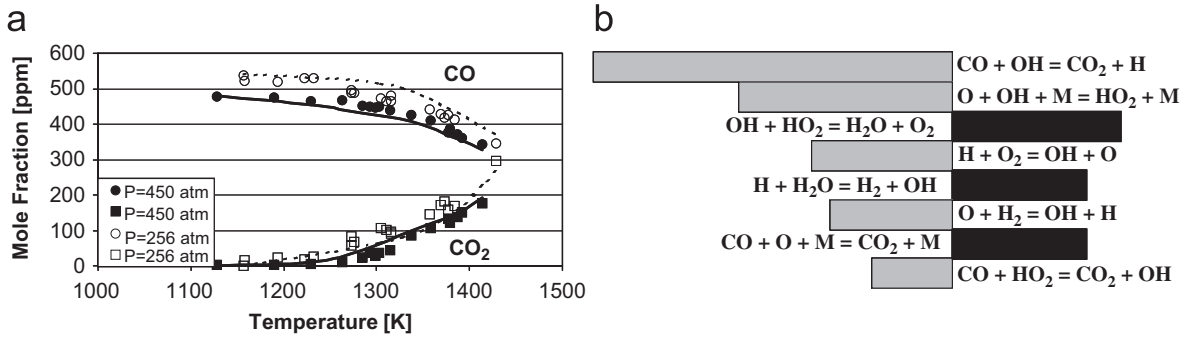

Fig. 6. Oxidation of CO/H_2 mixtures in a shock tube reactor at 256 and 450 atm. Panel (a). Calculated (lines) and experimental (symbols) [49] species profiles. Panel (b). Maximum sensitivity coefficients for [CO] in the conditions of panel (a) at 1400 K and $P = 450$ atm. Dark bars correspond to positive coefficients.

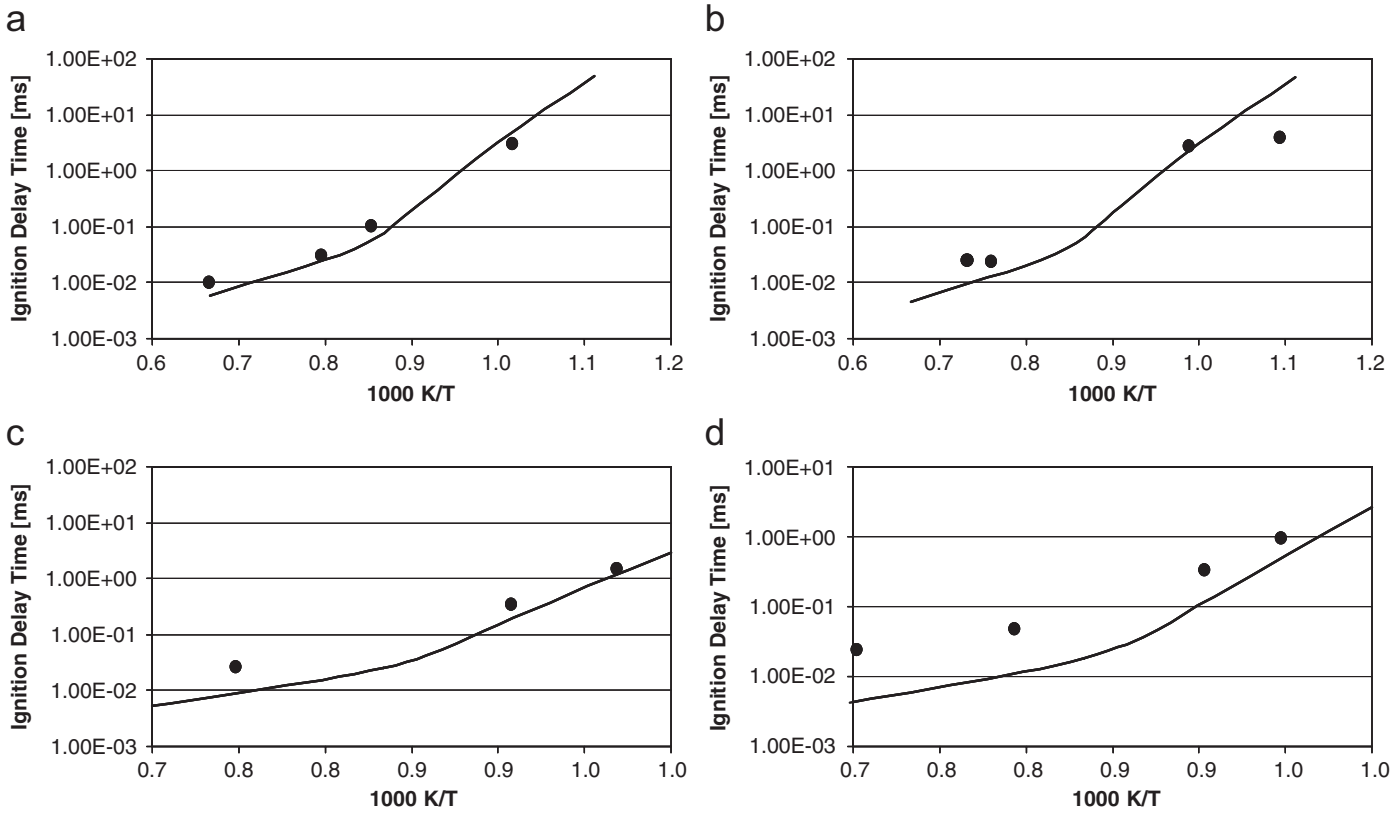

Fig. 7. Ignition delay times of different CO/H_2 mixtures at 10 atm. $CO : H_2 = 0 : 10$ (Panel (a)); 2.5:7.5 (Panel (b)); 5:5 (Panel (c)); 7.5:2.5 (Panel (d)). Comparison between predicted ignition delay times and experimental data [50].

predictions agree well with measurements at very high pressures too. CO concentration is sensitive to reactions involving HO_2 even in the high temperature range because of the high pressures. The sensitivity analysis as reported in Fig. 6b shows that, together with the more typical sensitive reactions, a couple of third body reactions ($O + OH + M = HO_2 + M$ and $CO + O + M = CO_2 + M$) play a significant role in justifying the reactivity of the system. In fact, the first reaction contributes to ruling HO_2 concentration while the second is a chain termination. Xia's [50] shock tube experiments measured the ignition delay times of various syngas mixtures in Argon at 10 atm. The molar composition Fuel:O_2 : Ar = 10 : 5 : 85 was kept constant in this study while the CO/H_2 ratio was systematically varied. Fig. 7 shows that model predictions agree with the experimental measurements, although the model underpredicts the induction times at high CO/H_2 ratios. The kinetic analysis confirms that the ignition times in these experiments are dominated by hydrogen chemistry and once again controlled by the competition between the chain branching ($H + O_2 = OH + O$) and the slow chain propagation reactions ($H + O_2 + M = HO_2 + M$).

Recently, Kalitan and Petersen [11,51] studied the ignition of CO/H_2–lean mixtures in air in a shock-tube device at

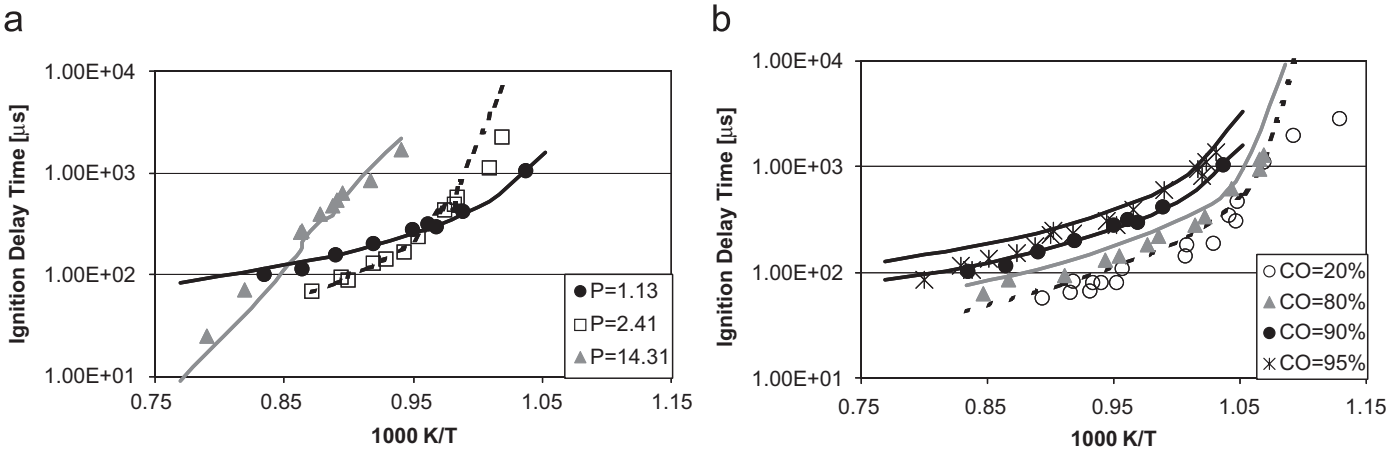

Fig. 8. Ignition delay times of CO/H_2-lean mixtures in air at $\Phi = 0.5$. Panel (a). Pressure effect (90%CO–10%H_2) [51]. Panel (b). Effect of fuel composition at near atmospheric conditions (20% CO–80% H_2, 80% CO–20% H_2, 90% CO–10% H_2 and 95% CO–5% H_2 [11]). Comparison between predicted (lines) and experimental ignition delay times (points).

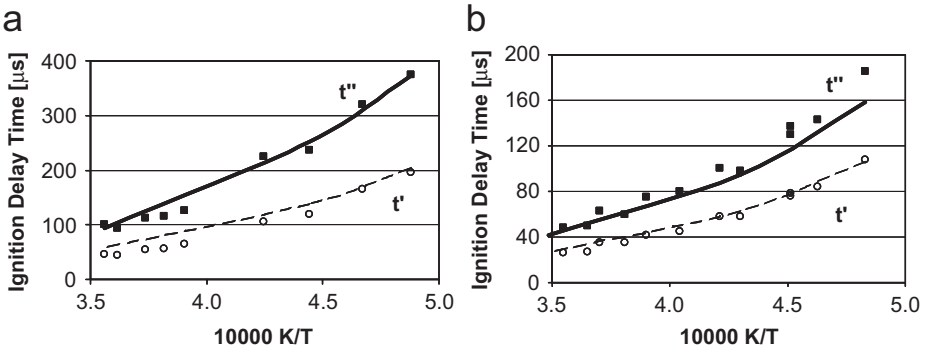

Fig. 9. Comparison between predicted ignition delay times and experimental data [45]. Panel (a). 0.049% H_2, 1.01% O_2, 3.28% CO, balance Ar; Pressure 1.23–1.91 atm. Panel (b). 0.005% H_2, 1.0% O_2, 12.17% CO, balance Ar; Pressure 1.4–2.2 atm.

900–1300 K and 1–15 atm. They also successfully compared the experimental measurements with the mechanism of Davis et al. [10] while the GRI30 [52] overestimated the ignition delays at low temperatures. Fig. 8 shows a comparison of these data [11] with the ignition delay times predicted by the mechanism of Table 1.

Fig. 8a shows the effect of pressure on the ignition time of a 90/10 CO/H_2 mixture. The pressure reduces the reactivity of the system at low temperatures. Reactivity actually increases, however, with pressure at higher temperatures. The model accurately captures this reverse behavior. The mechanism is indeed able to capture the change in the activation energy of the process from low to high temperatures under these conditions which are typically of interest in gas turbine operation.

Fig. 8b compares the induction delay times at different CO fractions in the fuel at ambient pressure. Higher amounts of CO in the fuel increase induction times. At temperatures lower than 900 K the model fails to fully explain the reactivity observed. Similar deviations were also partially observed, although not in a systematic way, when studying pure H_2 oxidation [9], and thus further experimental and modeling activities are required. It is important to emphasize that this low temperature discrepancy disappears at high pressures where HO_2 chemistry plays an important role.

Dean et al. [45] determined the ignition delay times of different H_2/CO mixtures in argon using both oxygen and nitrous oxide as the oxidizing agent at 2000–2850 K and 1.2 to 2.2 atm. Two different ignition delays (t' and t'') were derived from the measured profiles of CO_2 concentration. Fig. 9 shows the comparisons with both the ignition delay times for two different H_2/CO mixtures in rich (panel a) and very rich conditions (panel b). The sensitivity analysis in both the cases confirmed that the first time (t') is strongly dependent on H_2 reactions ($O + H_2 = OH + H$) while the oxidation reaction CO+OH becomes relevant for the second time.

The use of N_2O as the oxidant modifies the reactivity of the system. As already discussed elsewhere [9], N_2O readily produces O and OH radicals through the reactions $N_2O + M = N_2 + O + M$ and $N_2O + H = N_2 + OH$. Experimental measurements, as reported in Fig. 10, clearly show a minimum in the second induction time t'' at about 2400 K. Model predictions agree fairly well with this minimum delay time. This

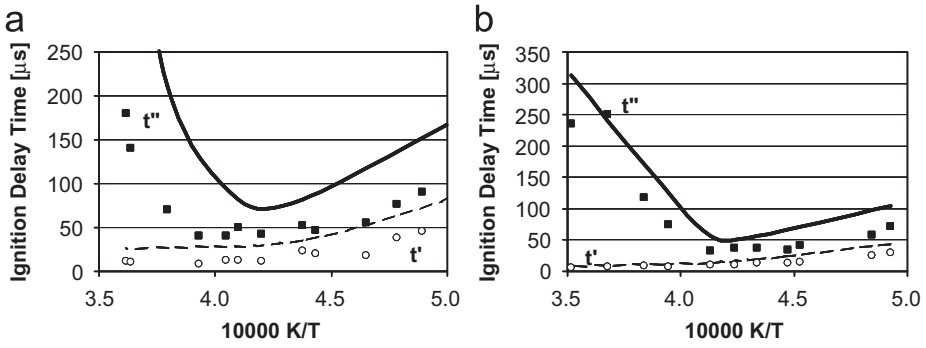

Fig. 10. Comparison between predicted ignition delays and measurements [45]. Panel (a). 0.05% H_2, 1.01% N_2O, 2.99% CO, balance Ar; $P = 1.15$–1.90 atm. Panel (b). 0.049% H_2, 1.04% N_2O, 12.01% CO, balance Ar; $P = 1.37$–2.21 atm.

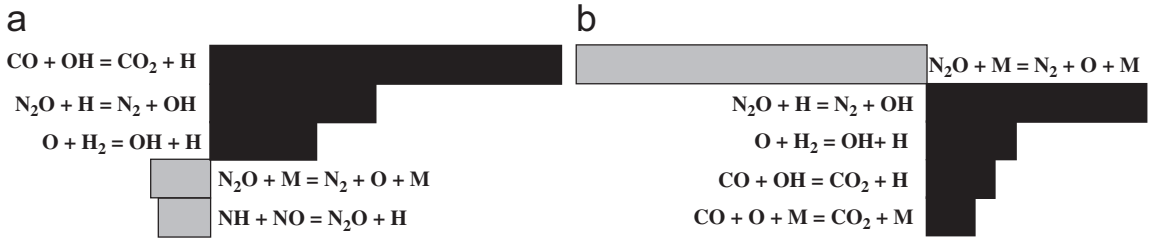

Fig. 11. Sensitivity coefficients of $[CO_2]$ concentration at time t''. Panel (a). Conditions of Fig. 10a at $T = 2285$ K. Panel (b). Conditions of Fig. 10a at $T = 2635$ K.

particular phenomenon depends on the competition between the two decomposition paths of N_2O to form O or OH radicals. In fact, the activation energy to form O is about 3 times higher than the one to form OH. Thus, the formation of O over OH is favored at temperatures higher than 2400 K. Thus, the OH/O ratio from N_2O decomposition is ~2 at 2200 K and ~0.5 at 2600 K. Fig. 11 shows a sensitivity analysis performed at two different temperatures. At relatively low temperatures (Fig. 11a), CO_2 formation is mainly sensitive to the CO+OH reaction while at high temperatures (Fig. 11b), CO oxidation is controlled by the competition between O and OH formation from N_2O decomposition.

The oxidation of CO through the $CO + OH = CO_2 + H$ reaction is faster than the chain terminating $CO + O + M = CO_2 + M$. At high temperatures, the increased O formation would favor CO conversion but the slow recombination reaction CO+O+M becomes the rate limiting step. For this reason the system exhibits a minimum at about 2300 K and the reactivity of the system decreases as the temperature increases. It is worth noting that these results, which were not observed with the previous Tsang and Hampson parameters [23], are obtained with the new rate constant of $CO + O + M = CO_2 + M$. In fact, as shown in Fig. 2, there is a reduction of the rate constant at high temperatures with these parameters.

3.3. Ignition in counterflow configuration

Fotache et al. [53] studied the ignition of various syngas mixtures with air in a counterflow configuration at different strain rates and pressures. In the experimental activity the temperature of the air stream was increased gradually to approach ignition while the air flow was simultaneously adjusted to maintain the momentum balance between the jets. The computational procedure parallels the experiments, and ignition can be achieved in a similar way by increasing the boundary air temperature. The addition of hydrogen strongly affects the reactivity of the system, especially at low concentrations ($H_2 < 5\%$). At high H_2 levels, after a transition zone, the ignition temperatures are nearly constant and the reactivity is ruled by the competition between $H + O_2 + M = HO_2 + M$ and $H + O_2 = OH + O$. Fig. 12 shows the comparison between model predictions and experimental measurements, and a sensitivity analysis performed for a nearly pure CO flame. Although hydrogen chemistry is important in this case, the competition between CO+OH and CO+O also plays a major role.

3.4. Laminar burning belocity

The kinetic mechanism is also tested against several experimental data relating to laminar burning velocities of different syngas mixtures at both atmospheric [54–59] and high pressures [21].

Fig. 13a shows the comparison between experimental measurements and model-predicted flame speeds. The position of the maximum speed at $\Phi \cong 2$ as well as the effect of CO content in the mixture are correctly predicted, only a slightly underestimation is observed at high hydrogen content. As expected and reported in Fig. 13b, flame speed increases significantly at

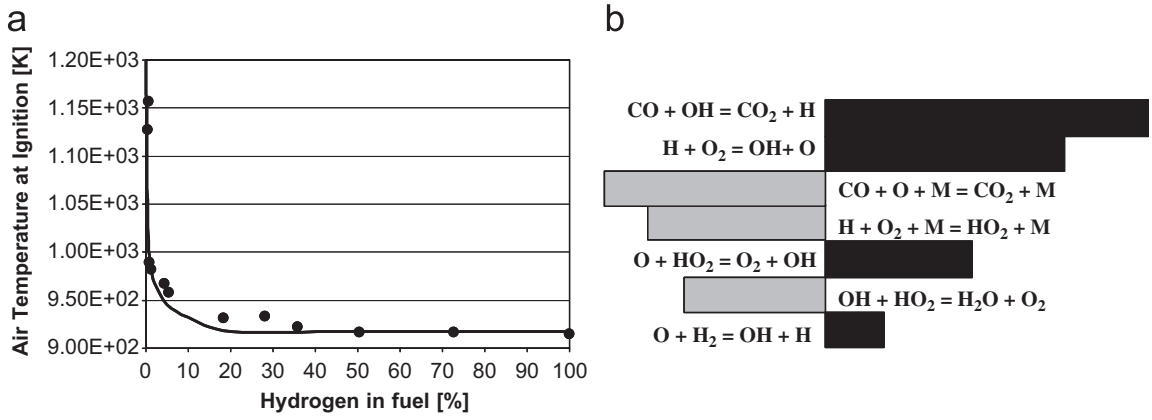

Fig. 12. Ignition temperatures as a function of H_2 concentration in the fuel in a counterflow diffusion flame at 1 atm and strain rate 100 s^{-1}. Panel (a). Comparison between experimental measurements (symbols) [53] and model prediction (line). Panel (b). Sensitivity analysis for temperature at conditions close to autoignition for a CO flame with 50 ppm of H_2. Dark bars correspond to positive sensitivity coefficients.

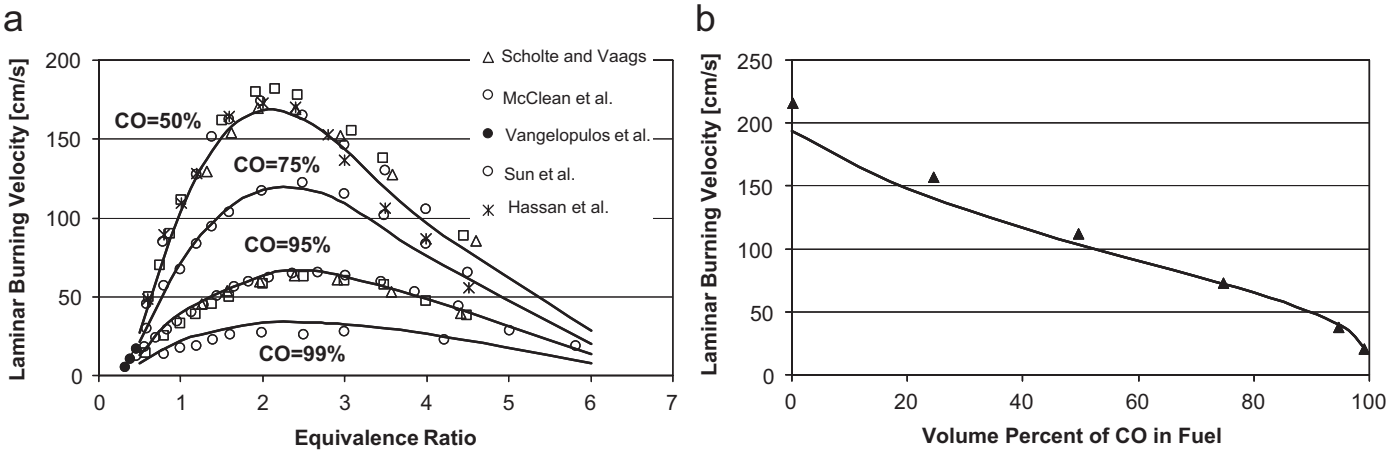

Fig. 13. Laminar flame speed of syngas in air at 1 atm and 298 K. Comparison between predicted and measured values [21,54–57]. Panel (a). Effect of flame stoichiometry. Panel (b). Effect of fuel composition at $\phi = 1$ [55].

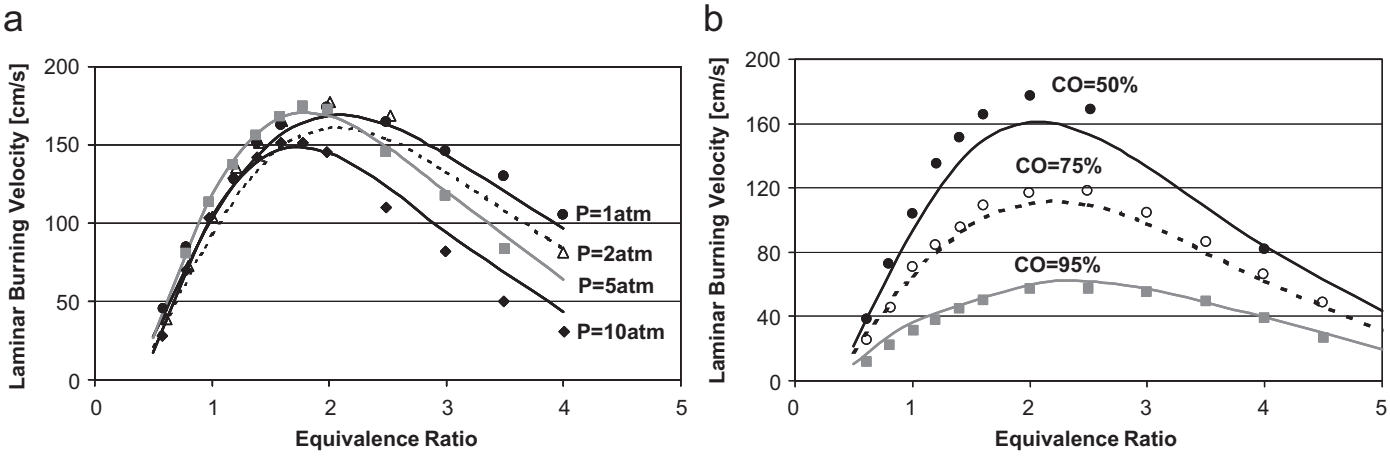

Fig. 14. Laminar flame speed of syngas at 298 K [21]. Panel (a). $CO/H_2 = 1$ in air ($P = 1$ and 2 atm) and in diluted conditions $He/O_2 = 7$ ($P = 5$ and 10 atm). Panel (b). Effect of syngas composition at $P = 2$ atm. Comparison between predicted and measured velocity.

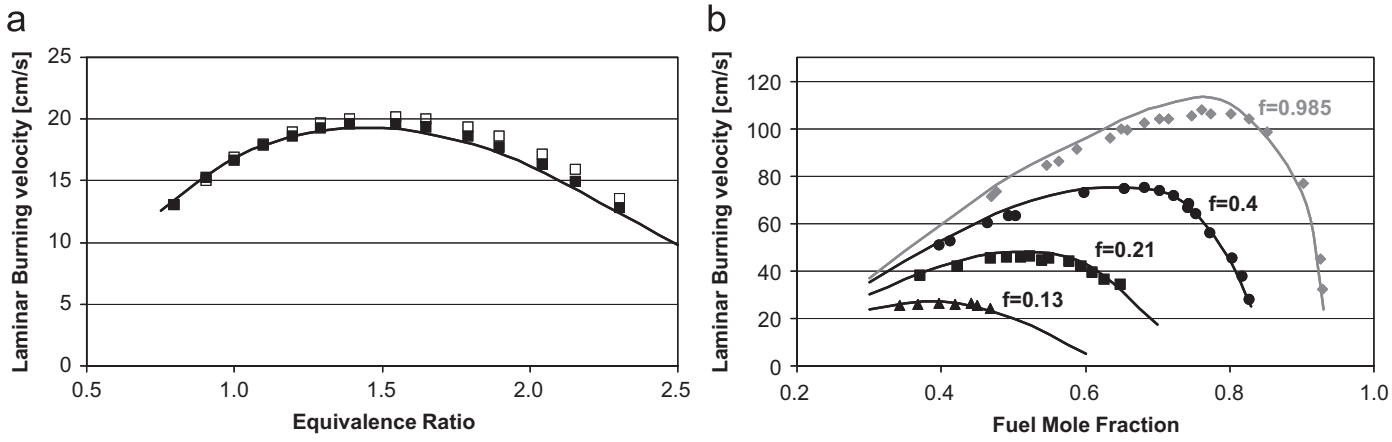

Fig. 15. Laminar flame speed of syngas at 1 atm. Panel (a). Syngas in air ($H_2 = 5.05\%$, $CO = 44.75\%$ $CO_2 = 50.2\%$) [58]. Panel (b). Effect of oxidant dilution on the flame velocities of CO with trace amounts of H_2 and H_2O [59]. Comparison between predicted (solid lines) and measured flame speeds (points). The two marks refers to two replicated experiments.

high H_2 concentrations and approaches zero for nearly pure CO flames in stoichiometric conditions. When the hydrogen concentration is high, the reactivity of the system is controlled by the competition between the reactions producing and consuming OH radicals. Flame speed is controlled by CO oxidation only at CO concentrations greater than ~95%.

Fig. 14 shows the effect of pressure and composition on syngas flame speed. Both these effects are correctly reflected by the model. Minor underestimations, systematically consistent with the previous data of Fig. 13a, are still observed at $\Phi = 2$ but only at low pressure. The different behavior of the high-pressure flames (5–10 atm) in Fig. 14a is essentially due to dilution with He, which was used during the experiment to increase the mixture's Lewis number and reduce cellular instabilities.

Further comparisons with the flame speed measurements of Konnov et al. [58] and Lewis and Von Elbe [59] are reported in Fig. 15. The first set of data [15] refers to the air oxidation of a syngas containing a large amount of CO_2 ($H_2 = 5.05\%$, $CO = 44.75\%$ and $CO_2 = 50.2\%$) at 298 K. Maximum flame speed occurs at slightly rich conditions. The second set of data [59] analyses the effect of O_2 concentration in the oxidant up to oxy-combustion conditions. The dilution factor is defined as $f = [O_2]/([O_2] + [N_2])$. Model predictions agree well with the experiments in these conditions too. Only a minor overestimation is observed for oxy-combustion in lean conditions.

4. Validation of the H_2–CO–NO_x kinetic scheme

The chemistry of nitrogen components and their interactions with hydrogen and hydrocarbon fuels in a wide range of temperature conditions have already been discussed in the literature, and a detailed kinetic scheme has been validated [9,36,37]. This kinetic scheme, coupled with the H_2–CO–O_2 scheme of Table 1, is discussed in further detail here and validated by comparison with the new experimental data already summarized in Table 3.

4.1. Premixed rich $CO/H_2/N_2O$/Ar flame

Vandooren et al. [60] studied a rich $H_2/CO/N_2O$/Ar flame at low pressure, to investigate the NO_x kinetics mechanisms in flames and to evaluate the effect of CO on the rate of N_2O reactions as the latter is typically used as an oxidizer for propellants. The structure of a similar flame (H_2/N_2O/Ar), both pure and NH_3-doped, was investigated by Sausa et al. [61] and has already been discussed in a previous paper [9]. This study confirms that at moderate temperatures the main reaction consuming N_2O is $N_2O + H = N_2 + OH$, as already discussed when analyzing Dean et al.'s data [45]. Moreover, NO is a minor primary product, formed through $N_2O + H = NH + NO$ with a selectivity of about 6%. Of course, CO is consumed through $CO + OH = CO_2 + H$. Fig. 16 shows the comparison between model results and experimental data. The slight NO underprediction seems a good compromise with the comparable NO overprediction when analyzing similar data in the H_2/N_2O systems [9].

4.2. The effect of NO_x addition to CO/H_2 mixtures

The effect of NO on the oxidation of syngas mixtures has been studied at nearly atmospheric pressure and temperatures ranging from 800 to 1400 K. Experiments were performed in a plug flow reactor by Glarborg et al. [47] and more recently in a jet stirred reactor at various equivalence ratios by Dagaut et al. [48]. The addition of NO promotes the oxidation of the CO/H_2 mixture at low temperatures ($T < 1000$ K) because HO_2 is rapidly transformed into the reactive OH radical through the reaction $NO + HO_2 = NO_2 + OH$. This accelerating effect is of particular interest since NO_x is commonly present in vitiated airstreams and even small amounts of NO will modify the reactivity of the system. Moreover, these measurements represent a useful way of further validating pure syngas oxidation.

Fig. 17 shows the comparison between model results and experimental measurements in a jet stirred reactor at different

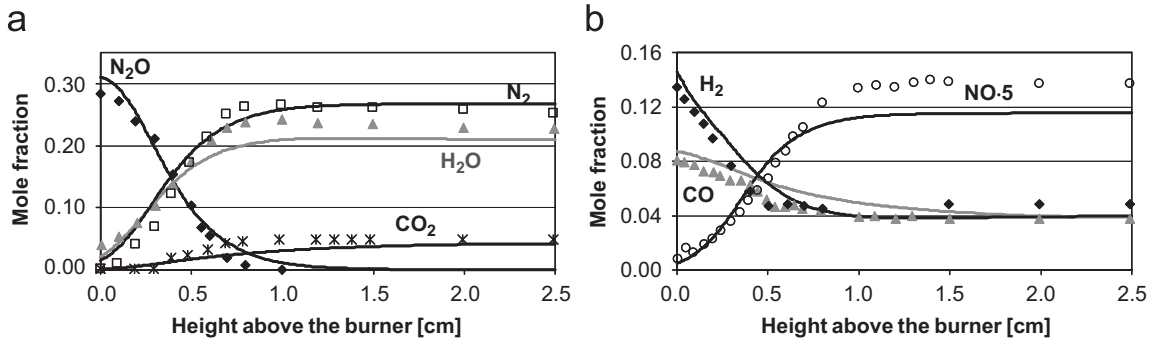

Fig. 16. Premixed syngas flame at 30 torr [60]. Molar composition: $H_2 = 0.258$, $CO = 0.082$, $N_2O = 0.284$, $Ar = 0.376$. Calculated (lines) and experimental (symbols) mole fractions.

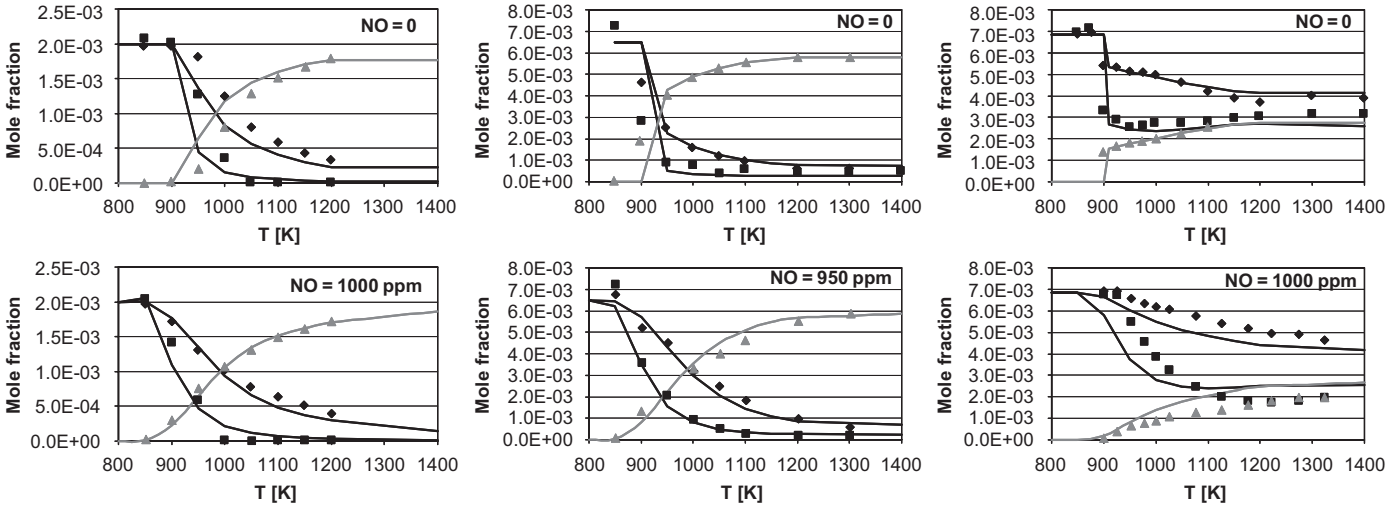

Fig. 17. Comparison between experimental (symbols) [48] and predicted species profiles (lines) at various equivalence ratios. $P = 1$ atm, residence time = 120 ms. Fuel lean conditions: $CO = H_2 = 2000$ ppm; Stoichiometric conditions: $CO = H_2 = 6500$ ppm; Fuel rich conditions: $CO = H_2 = 6850$ ppm, balance N_2.

equivalence ratios. In general, the model is able to simulate the measured profiles and to capture the effect of NO addition quite well. Under fuel–lean conditions, NO enhances the oxidation below 1000 K whereas it inhibits the reactivity of the system under stoichiometric and particularly under fuel rich conditions. This is a consequence of the growing importance of chain-termination reactions involving NO. In fact, at low temperatures (below 1000 K) and in fuel–lean conditions, the net effect of NO addition is to increase the reactivity of the system via the chain propagation reaction $NO + HO_2 = NO_2 + OH$. In fuel rich conditions, on the other hand, because of the higher concentration of H radicals, NO acts as a radical scavenger mainly through the reaction sequence $NO + H + M = HNO + M$ and $HNO + H = NO + H_2$ which corresponds to H-radical recombination ($H + H = H_2$).

The oxidation of moist CO ($H_2O = 1$–10%) at ~1000 K with NO addition up to 1400 ppm (residence times = 50 − 250 ms) was studied in a flow reactor by Glarborg et al. [47]. The results, shown in Fig. 18, highlight the enhancing role of NO on CO conversion at low NO concentrations. The addition of ~100 ppm shifts the reactivity of about 100 K towards lower temperatures by converting HO_2 to OH radicals. At higher concentrations, NO favors radical recombination reactions thus inhibiting CO oxidation. The recombination reaction $NO + O + M = NO_2 + M$ and the sequence $NO + OH + M = HONO + M$ followed by $HONO + OH = NO_2 + H_2O$ strongly reduce the system's reactivity. This effect is more pronounced at low H_2O content due to the small concentration of H and OH and the greater importance of O radicals. Rate parameters suggested by Skreiberg et al. [62] for the reaction $HONO + OH = NO_2 + H_2O$ were adopted to improve model predictions.

4.3. Ammonia chemistry and the SNCR process

Under favorable operating conditions, NH_3 selectively converts NO to N_2. This is used in practice in the thermal deNOx process by adding ammonia, urea and similar compounds to flue gases to remove NO. The chemistry of NH_3–H_2 systems is thus relevant to the understanding and optimization of the selective non-catalytic reduction (SNCR) technology.

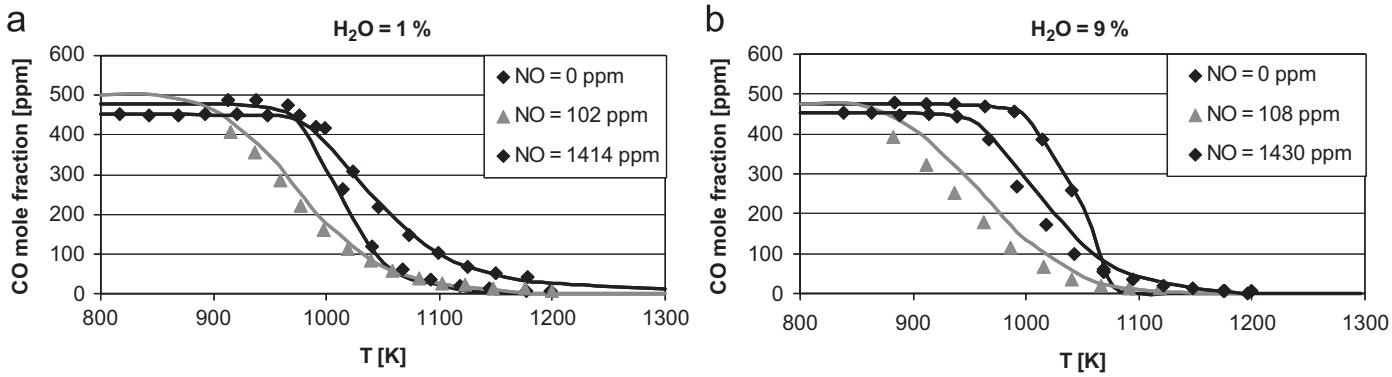

Fig. 18. Comparison between experimental (symbols) [47] and predicted species profiles (lines) at various NO additions. $P = 1.05$ atm, CO $\approx$ 500 ppm, $O_2 \approx 4\%$, balance N_2.

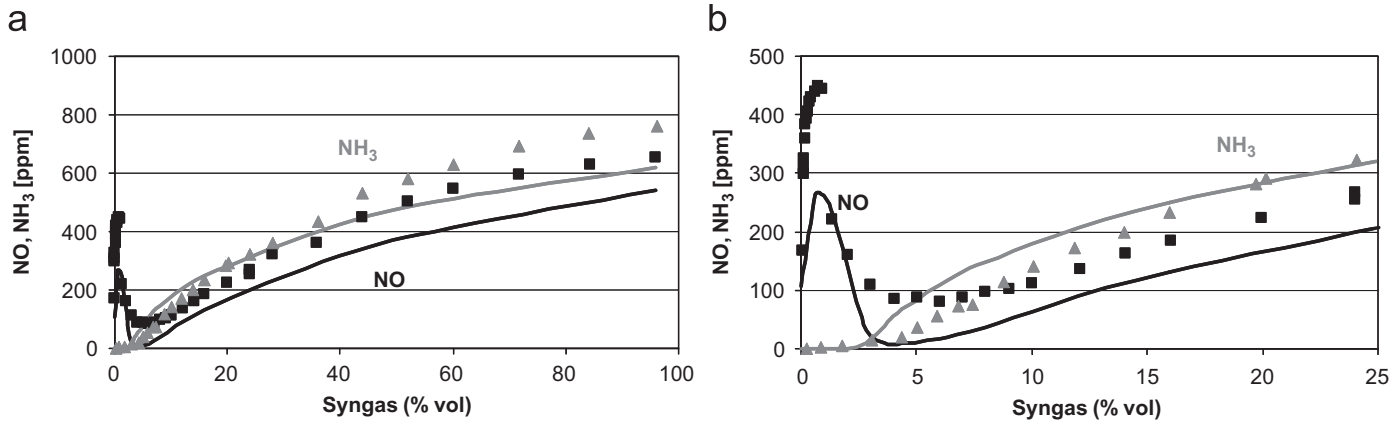

Fig. 19. Reduction of NO_x in SNCR conditions at ~1273 K and 1 atm. Inlet composition: syngas and N_2 with 1000 ppm of NO, 1000 ppm NH_3, 5000 ppm O_2. Panel (b) is a magnification in the optimal SNCR conditions. Comparison of experimental [63] and predicted (lines) concentrations.

This process is based on the reaction sequence $NH_3 \rightarrow NH_2 \rightarrow NH \rightarrow N$ which forms NH_i radicals capable of reducing NO to N_2($NH_2 + NO = N_2 + H_2O$, $NH + NO = N_2 + OH$).

Moreover, ammonia is a volatile product of organic nitrogen compounds in biomass fuels and can also be formed during coal pyrolysis.

Hasegawa and Sato [63] studied the SNCR condition in a non-isothermal flow reactor at moderate temperatures and atmospheric pressure. A fixed mixture of 1000 ppm NO, 1000 ppm NH_3 and 5000 ppm O_2 is fed to the reactor with a variable amount of syngas: $CO/H_2 = 3$. The effective contact time at high temperatures is in the order of about 1–2 s. Fig. 19 shows the conversions of NO and NH_3 as a function of the syngas in the feed. The behavior of NO and NH_3 is reasonably predicted over the full range of conditions. The CO presence does not significantly modify the results already discussed and analyzed in the previous paper [9]. NO reduction is slightly more effective than NH_3 conversion, mainly due to different reduction processes. Under the optimal conditions of the SNCR process, NO_x reduction efficiency is greater than 90% and the model over predicts this efficiency. However, the model correctly estimates the relative effect of NH_3 with respect to NO.

To further investigate SNCR conditions and model predictions, the same NO–NH_3–O_2 stream was also analyzed at ~1273 K with pure CO, in the absence of H_2. Fig. 20a shows that the model properly predicts the experimental trends, but NO reduction is still overpredicted at high CO levels. Note that only at low CO levels, i.e. in a fuel–lean system, the conditions correspond to those of SNCR. In the absence of CO, about 84% of the NO is reduced to N_2 while only ~50% is converted at about 1% CO. In fact, small CO addition enhances the radical pool concentration, the overall oxidation rate and the oxidation of ammonia radicals NH_i to NO. Higher amounts of CO make the system increasingly fuel rich and ammonia oxidation becomes less competitive.

The interaction NO–NH_3 was investigated by Hasegawa and Sato [63] by varying the NO addition to the reacting system. Fig. 20b shows the very good comparison between model results and experimental measurements. The NO concentration remains very low as long as the initial NO/NH_3 is lower than one. Moreover, higher amounts of NO facilitate NH_3 oxidation.

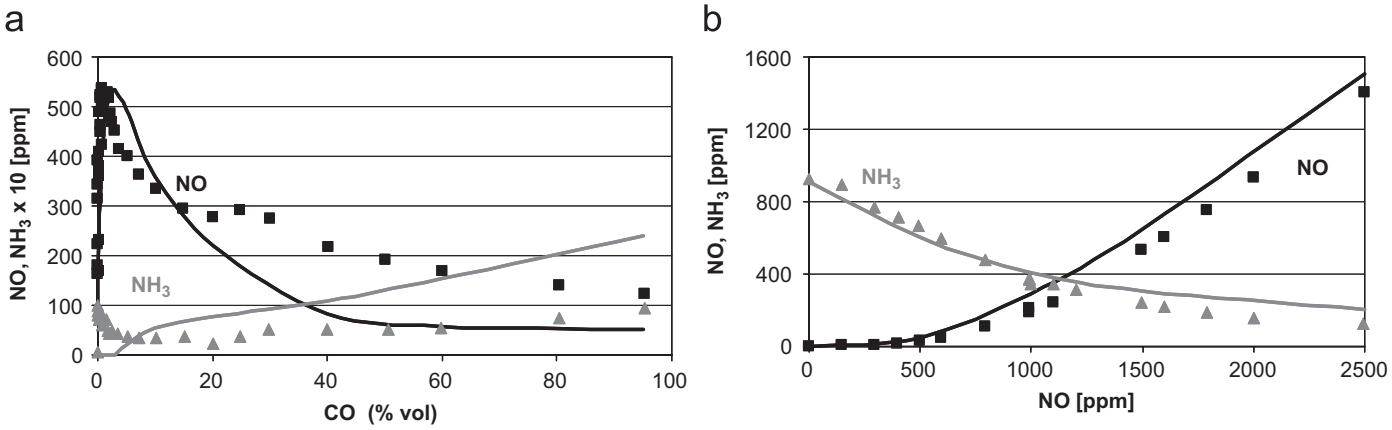

Fig. 20. Reduction of NO_x in SNCR conditions at ~1273 K and 1 atm. Panel (a). Inlet composition: CO and N_2 with 1000 ppm of NO, 1000 ppm NH_3, 5000 ppm O_2. Panel (b). Inlet composition: NO and N_2 with CO 0.24, H_2 0.091, 1000 ppm NH_3, 5000 ppm O_2. Comparison of experimental [63] and predicted (lines) concentrations.

5. Conclusions

The present study systematically revised a detailed kinetic scheme of oxidation and combustion of CO/H_2 mixtures with particular focus on interactions with nitrogen species and NO_x formation. Several recent and old experimental measurements were analyzed critically and compared with the predictions of the kinetic model.

In line with recent literature indications [10], rate parameters for the reaction $CO + OH$ were updated.

In a similar way, ignition delay times [45] and the high-pressure data [21,32,49] suggested new values for the reaction $CO + O + M$.

Rate parameters suggested by Skreiberg et al. [62] for the reaction $HONO + OH = NO_2 + H_2O$ were adopted to improve model predictions.

This paper offers a critical collection of experimental data and, more importantly still, a definition of a reliable kinetic scheme capable of simulating the combustion of syngas mixtures and the formation of pollutant species across a wide range of conditions, with particular emphasis on high pressures.

The same kinetic scheme is successfully applied to turbulent diffusion flames in a second note belonging to this paper. In the said note, a kinetic postprocessor is applied and coupled with CFD codes to investigate flame structures and pollutant formation in further detail.

Acknowledgements

This work was financially supported by ENEL and ENEA.

References

[1] Wender I. Fuel Process Technol 1996;48:189.
[2] Wu KT, Lee HT, Juch CI, Wan HP, Shim HS, Adams BR. et al. Fuel 2004;83:1991.
[3] Moliere M. ASME Paper # GT-2002-30017.
[4] Mittal G, Sung C-J, Yetter RA. Int J Chem Kinet 2006;38:516.
[5] Chiesa P, Macchi E. Trans ASME J Eng Gas Turb Power 2004;126(4):770.
[6] Miller JA, Pilling MJ, Troe J. Proc Combust Inst 2005;30:43.
[7] Ó Conaire M, Curran HJ, Simmie JM, Pitz WJ, Westbrook KJ. Int J Chem Kinet 2004;36(11):603.
[8] Li J, Zhao Z, Kazakov A, Dryer FL. Int J Chem Kinet 2004;36(10):566.
[9] Frassoldati A, Faravelli T, Ranzi E. Int J Hydrogen Energy 2006;31(15):2310.
[10] Davis SG, Ameya VJ, Wang H, Egolfopoulos F. Proc Combust Inst 2005;30:1283.
[11] Kalitan DM, Petersen EL. 41st AIAA/ASME/SAE/ASEE joint propulsion conference and exhibit, 10–13 July 2005, Tucson, Arizona (USA), paper 2005-3767; 2005.
[12] Saxena P, Williams FA. Combust Flame 2006;145:316–23.
[13] Walton SM, He X, Zigler T, Wooldridge MS. Proc Combust Inst 2006; 31.
[14] Kee RJ, Rupley F, Miller JA. The Chemkin thermodynamic data base, Sandia National Laboratories Report SAND89-8008, Livermore; 1989.
[15] Ranzi E, Sogaro A, Gaffuri P, Pennati G, Faravelli T. Combust Sci Tech 1994;96(4–6):279–325.
[16] Zhao Z, Li J, Kazakov A, Dryer FL, Int J. Chem Kinet 2005;37:282.
[17] Joshi AV, Wang H. Int J Chem Kinet 2006;38:57.
[18] Wooldridge MS, Hanson RK, Bowman CT. Proc Combust Inst 1994;25:741.
[19] Wooldridge MS, Hanson RK, Bowman CT. Int J Chem Kinet 1996;28:361–72.
[20] Golden DM, Smith GP, McEwen AB, Yu CL, Eitneer B, Frenklach M. et al. J Phys Chem A 1998;102:8598.
[21] Sun HY, Yang SI, Jomaas G, Law CK. Proc Combust Inst 2006; 31.
[22] Nist best fit, 2006, ⟨http://kinetics.nist.gov/index.php⟩.
[23] Tsang W, Hampson RF. J Phys Chem Ref Data 1986;15:1087.
[24] Lin MC, Bauer SH. J Chem Phys 1969;50:3377.
[25] Warnatz J. In: Gardiner Jr WC, editor. Combustion chemistry. New York: Springer; 1984.
[26] Hardy JW, Gardiner Jr. WC, Burcat A. Int J Chem Kinet 1978;10:503.
[27] Wagner HG, Zabel F. Ber Bunsen-Ges Phys Chem 1974;72:705.
[28] Inn ECY. J Chem Phys 1974;61:1589.
[29] Simonaitis R, Heicklen J. J Chem Phys 1972;56:2004.
[30] Toby S, Sheth S, Toby FS. The chemistry of combustion processes, In: Sloane TM, editor. ACS symposium series, vol. 249. Washington, DC; 1984. p. 267–76.
[31] Kondratiev VN. React Kinet Catal Lett 1974;1:7.
[32] Mueller MA, Yetter FL, Dryer FL. Int J Chem Kinet 1999;31:705.
[33] Kondratiev VN. Proc Combust Inst 1959;7:41.
[34] Allen MT, Yetter RA, Dryer FL. Combust Flame 1997;109:449.

[35] Troe J. Proc Combust Inst 1975;667:15.
[36] Faravelli T, Frassoldati A, Ranzi E. Combust Flame 2003;132:188.
[37] Frassoldati A, Faravelli T, Ranzi E. Combust Flame 2003;135:97.
[38] Barlow RS, et al. Sandia/ETH-Zurich $CO/H_2/N_2$ flame data—Release 1.1. ⟨www.ca.sandia.gov/TNF⟩, Sandia National Laboratories; 2002.
[39] Drake MC, Pitz RW, Correa SM, Lapp M. Proc Combust Inst 1984;20:1983.
[40] Buzzi Ferraris G, Manca D. Comp Chem Eng 1998;22(11):1595.
[41] Kee RJ, Grcar JF, Smooke MD, Miller JA. A Fortran program for modeling steady laminar 1-D premixed flames, Sandia National Laboratories Report. SAND85-8240;1985.
[42] Lutz AE, Kee RJ, Grcar JF, Rupley FM. OPPDIF: a fortran program for computing opposed flow diffusion flames, SAND96-8243, Sandia Report; 1997.
[43] Yetter RA, Dryer FL, Rabitz H. Combust Sci Technol 1991;79:129.
[44] Kim TJ, Yetter RA, Dryer FL. Proc Combust Inst 1994;25:759.
[45] Dean AM, Steiner DC, Wang EE. Combust Flame 1978;32:73.
[46] Alzueta MU, Bilbao R, Glarborg P. Combust Flame 2001;127:2234.
[47] Glarborg P, Kubel D, Dam-Johansen K, Chiang H, Bozzelli JW. Int J Chem Kinet 1996;28:773.
[48] Dagaut P, Lecomte F, Mieritz J, Glarborg P. Int J Chem Kinet 2003;35:564.
[49] Sivaramakrishnan R, Comandini A, Tranter RS, Brezinsky K, Davis SG, Wang H. Proc Combust Inst 2006; 31.
[50] Xia Y. PhD thesis, University of Wales, Aberystwyth;2000.
[51] Kalitan DM, Petersen EL, Mertens J, Crofton MW. ASME Paper GT2006-90488. Proceedings ASME turbo expo, May 8–11, Barcelona, Spain;2006.
[52] Bowman CT, Hanson RK, Davidson DF, Gardiner Jr WC, Lissianski V, Smith GP, et al. GRI-Mech, 2006, ⟨http://www.me.berkeley.edu/gri_mech/⟩.
[53] Fotache CG, Tan Y, Sung CJ, Law CK. Combust Flame 2000;120:417.
[54] Scholte TG, Vaags PB. Combust Flame 1959;3:511.
[55] McLean IC, Smith DB, Taylor SC. Proc Combust Inst 1994;25:749.
[56] Vagelopoulos CM, Egolfopoulos FN. Proc Combust Inst 1994;25:1317.
[57] Hassan MI, Aung KT, Faeth GM. J Propal Power 1997;13(2):239.
[58] Konnov AA, Dyakov IV, De Ruyck J. Proc Combust Inst 2002;29:2171.
[59] Lewis B, Von Elbe G. Combustion, flames, and explosions of gases, 3rd ed., New York; Academic Press; 1987. p. 398.
[60] Vandooren J, Van Tiggelen PJ, Pauwels J-F. Combust Flame 1997;109:647.
[61] Sausa RC, Singh G, Lemire W, Anderson WR. Proc Combust Inst 1996;26:1043.
[62] Skreiberg O, Kilpinen P, Glarborg P. Combust Flame 2004;136:501.
[63] Hasegawa T, Sato M. Combust Flame 1998;114:246.
[64] Timonen RS, Ratajczak E, Gutman D. J Phys Chem 1987;91:5325.
[65] Jachimowski CJ. Combust Flame 1977;29:55.